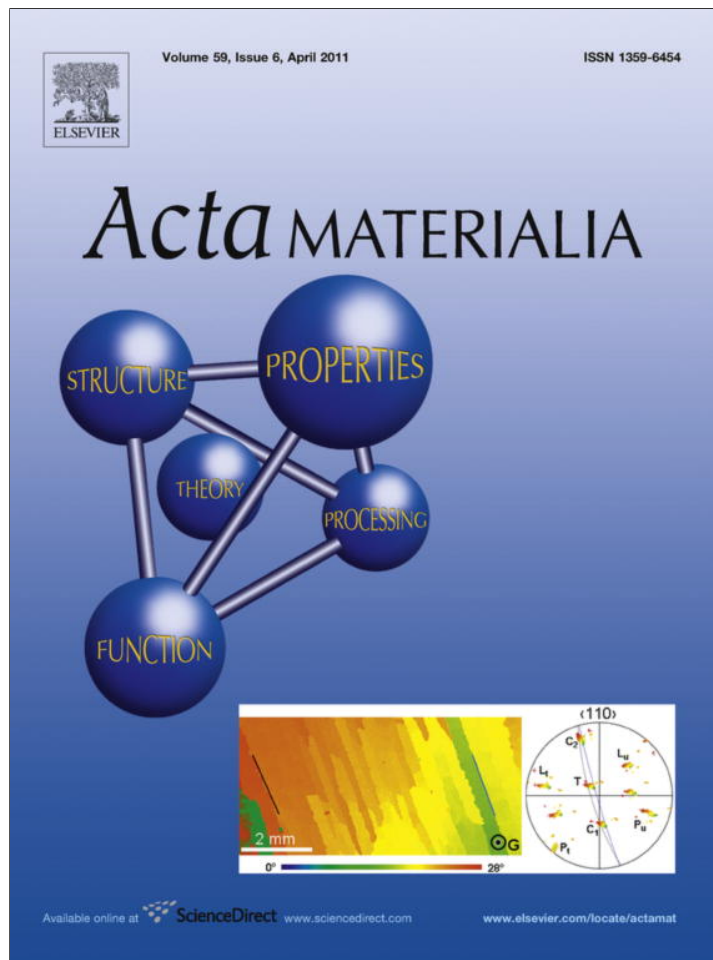


Provided for non-commercial research and education use.
Not for reproduction, distribution or commercial use.



This article appeared in a journal published by Elsevier. The attached copy is furnished to the author for internal non-commercial research and education use, including for instruction at the authors institution and sharing with colleagues.

Other uses, including reproduction and distribution, or selling or licensing copies, or posting to personal, institutional or third party websites are prohibited.

In most cases authors are permitted to post their version of the article (e.g. in Word or Tex form) to their personal website or institutional repository. Authors requiring further information regarding Elsevier's archiving and manuscript policies are encouraged to visit:

<http://www.elsevier.com/copyright>



Evolution of defects in copper deformed by high-pressure torsion

J. Čížek^{a,*}, M. Janeček^b, O. Srba^b, R. Kužel^c, Z. Barnovská^a, I. Procházka^a, S. Dobatkin^d

^a Faculty of Mathematics and Physics, Charles University in Prague, Department of Low Temperature Physics, V Holešovičkách 2, Prague 8, CZ-18000, Czech Republic

^b Faculty of Mathematics and Physics, Charles University in Prague, Department of Physics of Materials, Ke Karlovu 5, 12116 Prague 2, CZ-12116, Czech Republic

^c Faculty of Mathematics and Physics, Charles University in Prague, Department of Condensed Matter Physics, Ke Karlovu 5, 12116 Prague 2, CZ-12116, Czech Republic

^d A.A. Baikov Institute of Metallurgy and Materials Science, Russian Academy of Sciences, Moscow, Russia

Received 28 November 2010; received in revised form 14 December 2010; accepted 14 December 2010

Available online 13 January 2011

Abstract

Lattice defects in Cu deformed by high-pressure torsion (HPT) were investigated by positron annihilation spectroscopy (PAS) combined with transmission electron microscopy, X-ray diffraction (XRD) and Vicker's microhardness (HV) measurements. The evolution of the microstructure during HPT processing was studied on samples subjected to various numbers of HPT revolutions using pressures of 2 and 4 GPa. Since strain in torsion deformation increases with the radial distance from the center of rotation, one can expect a non-uniform microstructure across the sample diameter. To examine this, HV was measured at various distances from the center of the HPT-deformed sample and the microstructure at the center was compared with that at the periphery. It was found that HPT-deformed Cu contains a high density of dislocations and also small vacancy clusters formed by the agglomeration of deformation-induced vacancies. The center of the sample exhibits coarser grains, a slightly lower density of dislocations and smaller vacancy clusters compared to the periphery. The dislocation density and concentration of vacancy clusters were evaluated from the combination of the PAS and XRD results. The theoretically estimated concentration of deformation-induced vacancies is of an order of magnitude comparable to that determined in experiment.

© 2010 Acta Materialia Inc. Published by Elsevier Ltd. All rights reserved.

Keywords: Severe plastic deformation (SPD); High-pressure torsion; Lattice defects; Vacancies; Transmission electron microscopy (TEM)

1. Introduction

Ultrafine-grained (UFG) materials with a grain size below 1 μm exhibit a number of advantageous properties compared to traditional polycrystals [1]. In particular, UFG materials are characterized by a favorable combination of very high strength and enhanced ductility [1,2]. The main feature of (UFG) materials is the significant volume fraction of grain boundaries (GBs), which results in new, unusual physical properties, e.g. high diffusion activity [3] and superplasticity [4]. Bulk UFG materials with a

grain size typically around 100 nm can be prepared by high-pressure torsion (HPT) [1,5]. Severe plastic deformation applied during HPT processing introduces a large number of dislocations. Hence, lattice defects play an important role in UFG materials. The detailed characterization of these defects and their evolution during HPT processing is necessary for understanding the specific properties of UFG materials.

Defect studies of UFG Cu prepared by HPT were performed in this work, including (i) characterization of lattice defects introduced by HPT and (ii) investigation of defect evolution during HPT processing. Positron annihilation spectroscopy (PAS) is a well-developed non-destructive technique with a high sensitivity to open-volume defects,

* Corresponding author. Tel.: +420 2 2191 2788; fax: +420 2 2191 2567.
E-mail address: jakub.cizek@mff.cuni.cz (J. Čížek).

e.g. vacancies, dislocations and vacancy clusters [6]. In this work PAS was employed as a principal technique of defect characterization and was combined with X-ray diffraction (XRD) line-profile analysis and the direct observation of microstructure by transmission electron microscopy (TEM). Variations of mechanical properties were monitored by Vicker's microhardness (HV) measurements.

Previous TEM investigations of HPT-deformed Cu revealed a fragmented structure, with high-angle misorientation of neighboring grains and a high dislocation density [2,7,8]. Positron lifetime (LT) investigations of UFG Cu prepared by HPT revealed two types of defects [8]: (i) dislocations and (ii) small vacancy clusters with a size comparable to a few vacancies. There are indications that very high concentration of vacancies is created by severe plastic deformation [9–12]. Dislocation densities determined from measurements of the stored energy by differential scanning calorimetry (DSC) and residual electrical resistivity are three to four times higher than those obtained from XRD line-profile analysis. Several authors proposed that this discrepancy is due to excess vacancies, which also contribute to the total stored energy [10–12]. PAS enables the direct determination of the concentration of vacancies and can clearly distinguish between monovacancies and vacancy clusters. Hence, using PAS, one can determine whether UFG materials contain single vacancies or if deformation-induced vacancies have agglomerated and formed vacancy clusters.

In HPT processing a disk-shaped sample located between two anvils is subjected to compressive pressure of several gigapascals and simultaneously strained by a rotating anvil. The shear strain γ imposed on the disk during HPT performed using N revolutions can be estimated from the relationship [1,5]

$$\gamma = \frac{2\pi Nr}{h} \quad (1)$$

where h denotes thickness of the deformed sample and r is the sample radius. Hence, for a disk-shaped sample, the imposed strain increases with radial distance r , from zero at the disk center up to a maximum value at the edge. As a consequence, one can expect that the microstructure at the center differs from that at the periphery. Indeed, HV measurements performed across the diameter of HPT-deformed Cu [13] and Ni [14,15] revealed lower hardness at the center compared to the periphery. The difference between the center and the periphery becomes smaller with higher compressive pressure and higher number of turns. A relatively homogeneous HV profile across the sample was achieved using a combination of sufficiently high pressure and number of revolutions. These results agree well with strain gradient plasticity modeling of HPT processing [16]. Recent investigations of HPT-deformed Cu–Ag alloy [17] and high-purity Al [18] performed by scanning electron microscopy revealed that straining occurs initially at the periphery of the disk and with increasing strain the deformation spreads towards the center. Observations of vortex

microstructures were reported in Refs. [17,18], suggesting the occurrence of Kelvin–Helmholtz instabilities caused by a difference in the local shear velocity between adjacent positions. A variation in the concentration of small vacancy clusters with distance from the center was detected by PAS in UFG Cu subjected to 5 HPT turns under a pressure of 6 GPa [19]. This is another strong indication for non-homogeneity in defect concentration across the sample diameter.

2. Experimental

Technical-purity Cu (99.95 wt.%) specimens were subjected to quasi-constrained HPT straining at room temperature. Samples processed under two different compressive pressures (2 and 4 GPa) were compared. The evolution of the microstructure was investigated by the measurement of samples subjected to 1, 3, 5, 10, 15 and 25 HPT revolutions. HPT-deformed specimens were disk shaped, with a diameter of ~ 9 mm and a thickness of ~ 0.3 mm.

PAS investigations were performed using a fast-fast positron lifetime spectrometer [20] with a time resolution of 150 ps (FWHM ^{22}Na). At least 10^7 annihilation events were accumulated in each LT spectrum. A $^{22}\text{Na}_2\text{CO}_3$ positron source with diameter of ~ 3 mm and activity of ~ 1 MBq was used. The mean penetration depth of positrons emitted by this source into Cu amounts to ~ 30 μm . The source contribution representing a contribution of positrons annihilated in the $^{22}\text{Na}_2\text{CO}_3$ spot and the covering mylar foil consisted of two weak components with lifetimes of 0.368 and 1.5 ns and relative intensities of 8% and 1%.

TEM observations were carried out on a JEOL JEM 2000 FX electron microscope operating at 200 kV. Foils for TEM were prepared by electrolytic polishing in STRUERS TENUPOL 5 jet-polishing unit using 50% H_3PO_4 at 10 $^\circ\text{C}$.

XRD measurements were carried out with the aid of an X'Pert Pro powder diffractometer (PANalytical) using filtered Cu $\text{K}\alpha$ radiation. Detection of scattered X-rays was performed with a PIXCel position-sensitive detector (PANalytical). Line-profile analysis was done using the whole pattern fitting program MStruct described in Refs. [21,22], which was developed at the Charles University in Prague as an extension of the Fox code for structure solution from powder diffraction [23].

The HV was measured by STRUERS Duramin 300 hardness tester using a load of 100 g applied for 10 s.

3. Results and discussion

3.1. TEM

As shown schematically in Fig. 1A, foils for TEM investigations ($\varnothing = 3$ mm) were cut (i) from the center of the sample ($r = 0$) and (ii) from the periphery ($r = 3$ mm). TEM observations of the sample subjected to 1 HPT

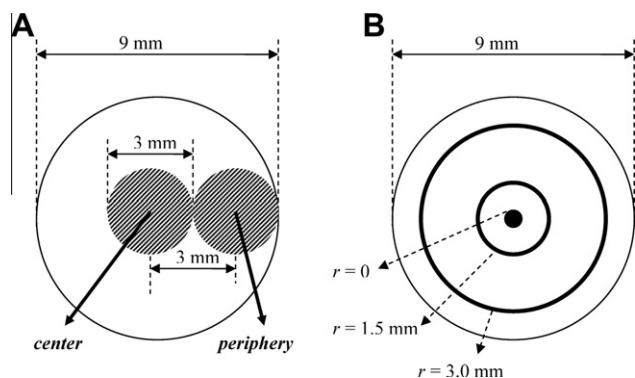


Fig. 1. Schematic illustration showing the regions in the sample investigated in this work. (A) Regions cut from the sample for preparation of the foils for TEM, i.e. the center region at $r = 0$ and the periphery region centered at $r = 3$ mm. The same regions were examined by PAS. (B) The circles at various distances from the center. The HV values shown in Fig. 4 were obtained by averaging the values measured on these circles: center ($r = 0$ mm), middle ($r = 1.5$ mm) and periphery ($r = 3.0$ mm).

revolution revealed a microstructure similar to that reported in Ref. [7], i.e. a heavily deformed structure with a high density of dislocations and a strong stress field both at the center and at the periphery. The microstructure at the center exhibits features typical of the initial stages of dislocation rearrangement, i.e. the formation of cells with lowered dislocation density separated by dislocation walls. On the other hand, a more refined microstructure was observed at the periphery.

Fig. 2A shows the microstructure at the center of a sample subjected to 15 HPT turns using a pressure of 4 GPa. The microstructure at the center consists of dislocation cells and sub-grains separated by tangled dislocations.

The periphery of the sample shown in Fig. 2B exhibits a refined structure with a mean grain size of 200–300 nm,

which is in reasonable agreement with the prediction of the second-order strain gradient model [16]. Hence, from TEM investigation it is clear that the microstructure at the center differs significantly from that at the periphery even after 15 HPT revolutions. This again agrees well with the second-order strain gradient model [16], which predicts a coarser structure at the center persisting even after 5 HPT turns.

3.2. Microhardness

The dependence of the microhardness on the radial distance r from the center is shown in Fig. 3 for Cu samples subjected to HPT under the pressure of 4 GPa. The center is characterized by a lower HV, the hardness increasing from the center towards the edge of the sample. With increasing number of HPT revolutions, the HV at the center increases and the difference between the center and the periphery becomes smaller.

Fig. 4 shows development of HV at three distances from the center shown schematically in Fig. 1B: (i) the center ($r = 0$ mm), the middle region ($r = 1.5$ mm) and the periphery ($r = 3.0$ mm). The periphery is already characterized by a high hardness ($HV \approx 150$) after the first HPT revolution. There is no systematic development of HV with increasing number of HPT turns except that statistical scattering can be seen at the periphery. On the other hand, in the middle region the HV increases with the number of HPT turns. In the sample subjected to 15 HPT turns, the HV in the middle region reached the value ($HV \approx 150$) typical of the periphery. This behavior indicates that the region characterized by higher hardness extends from the periphery towards the center with increasing number of HPT revolutions. HV in the center gradually increases with increasing number of HPT revolutions, testifying again that the

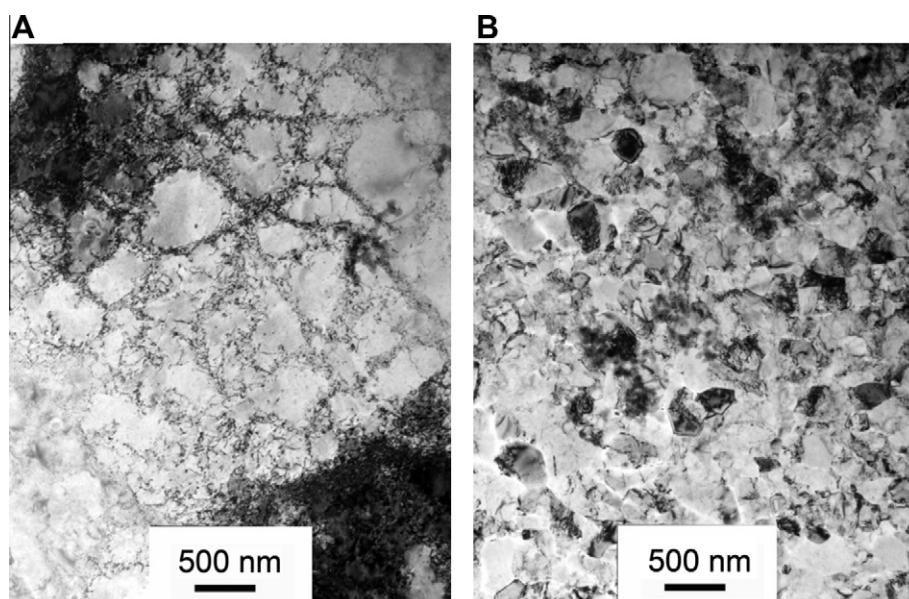


Fig. 2. A bright field TEM image of the sample subjected to 15 HPT turns: (A) center of the sample disk; (B) periphery of the sample.

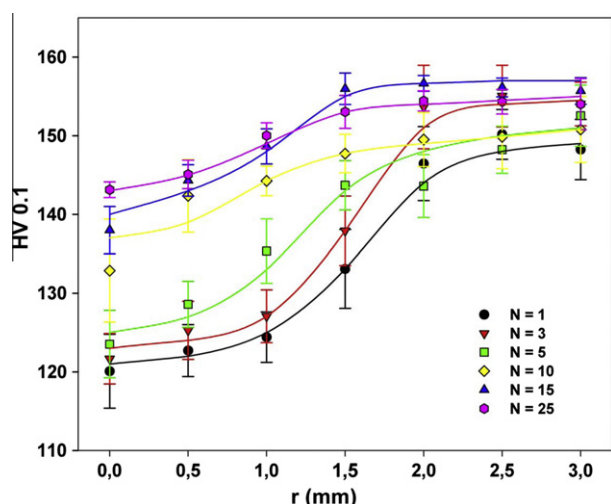


Fig. 3. Dependence of the microhardness HV on the radial distance r from the center of the sample disk. The data in the figure were measured on Cu subjected to various numbers of HPT revolutions under a pressure of 4 GPa. Each point is an average from several measurements performed at the same distance r from the center (except for the HV value at the center, $r = 0$).

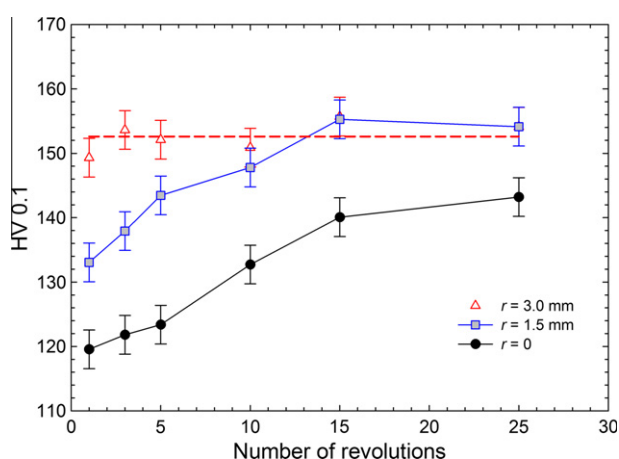


Fig. 4. Development of microhardness with increasing number of HPT turns in various regions: center ($r = 0$ mm), middle region ($r = 1.5$ mm) and periphery ($r = 3.0$ mm). In the middle region and the periphery, each point represents an average from several measurements performed at the same distance from the center.

region with higher hardness extends from the periphery towards the center. This is in accordance with the strain gradient modeling [16] and demonstrates that a reasonably homogeneous structure can be achieved after a sufficient number of HPT turns. However, even the sample subjected to 25 HPT turns exhibits an HV that is slightly lower at the center than at the periphery.

The formation of a region with increased HV propagating towards the center was also observed in recent investigations of HPT-deformed high-purity Al [18]. However, contrary to our results, the region with enhanced HV already extended to the center after 1 HPT revolution. Moreover, the Al sample exhibited dynamic recovery and

grain growth, which again started at the periphery and led to a softening. The recovered region propagated towards the center with increasing number of HPT turns. Complete homogenization with constant HV across the whole sample was achieved after 20 HPT turns. Hence, homogenization in HPT-deformed high-purity Al occurs faster than in the technical-purity Cu studied here. This could be due to the greater mobility of dislocations in Al, which leads to rapid recovery and enables homogeneity across the sample to be achieved more quickly than in Cu. The results in Ref. [18] indicate that constant HV across the whole Cu sample should also be achieved after a sufficient number of HPT revolutions.

3.3. XRD

The area illuminated by the X-ray beam covered the center of the specimen as well as the periphery. Therefore, both the center and the periphery contribute to the recorded diffraction pattern. The coherently scattering domain size, i.e. the mean size of dislocation-free domains corresponding approximately to the mean size of dislocation cells, and the dislocation density determined by XRD should therefore be regarded as an average over the whole sample. Note that no significant differences in the width of XRD reflections measured at the center and at the periphery were found in a Cu sample subjected to 10 HPT revolutions [19]. Fig. 5 shows the domain size plotted as a function of the number of HPT revolutions. Already after the first HPT revolution the domain size has reduced down to ~ 100 nm. After two HPT turns the domain size becomes approximately constant and basically does not change further with increasing number of HPT turns. Although the sample deformed using a pressure of 4 GPa exhibits slightly smaller domain size compared to that deformed using a pressure of 2 GPa, the general trend in development of domain size is similar in both samples. It should be mentioned that the domain size determined by

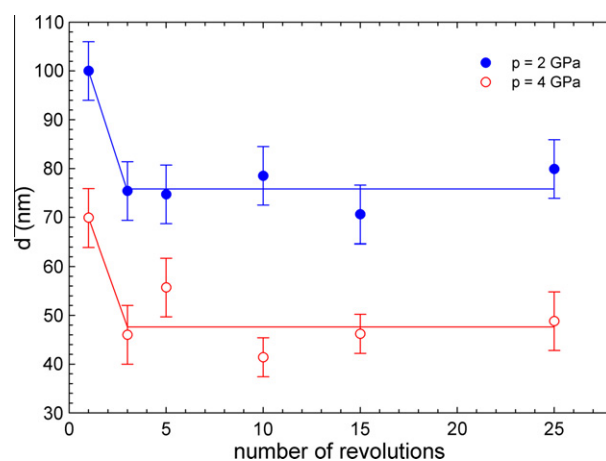


Fig. 5. The mean size d of coherently scattering domains determined by XRD line-profile analysis plotted as a function of the number of HPT revolutions.

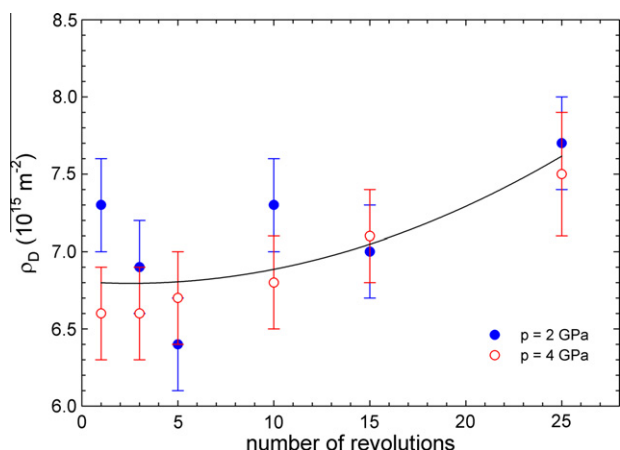


Fig. 6. The mean dislocation density ρ_D determined by XRD line-profile analysis plotted as a function of the number of HPT revolutions.

XRD is always smaller than the grain size estimated e.g. by TEM [8]. This is because XRD provides the mean size of coherently diffracting crystallites, i.e. regions with almost perfect structure and without microstrains, which are caused mostly by dislocations. Hence, contrary to grains discernible by TEM, coherently scattering domains are e.g. dislocation cells or sub-grains. These are not necessarily separated by well-defined GBs.

The mean dislocation density ρ_D determined by XRD line-profile analysis is plotted in Fig. 6 as a function of the number of HPT revolutions. The Cu samples deformed using pressures of 2 and 4 GPa both exhibit a high density of dislocations $\rho_D \approx 7 \times 10^{15} \text{ m}^{-2}$. This value is comparable to the dislocation density reported on HPT-deformed Cu and Ni [12,24] and is significantly higher than the dislocation density found in Cu deformed by equal channel angular pressing (ECAP) [10,11]. One can see in Fig. 6 that the mean dislocation density is almost saturated and shows only a very slight increase with increasing number of HPT revolutions.

3.4. PAS

LT spectra of HPT-deformed Cu samples are well fitted by two exponential components with lifetimes τ_1 and τ_2 and relative intensities I_1 and I_2 normalized so that $I_1 + I_2 = 100\%$. The evolution of lifetimes τ_1 , τ_2 with increasing number of HPT revolutions is plotted in Fig. 7. Both lifetimes τ_1 and τ_2 are significantly longer than the bulk positron lifetime in Cu $\tau_B = 114 \text{ ps}$ [8,19]. Hence, both components detected in HPT-deformed samples represent a contribution of positrons trapped at defects. The shorter component, with dominating intensity, exhibits a lifetime $\tau_1 \approx 164 \text{ ps}$, which agrees well with the lifetime of positrons trapped at dislocations in Cu [8,25]. Thus, dislocations created during severe plastic deformation represent the dominating type of defects in HPT-deformed Cu samples. The longer component, with lifetime τ_2 , can be attributed to positrons trapped in vacancy clusters (microvoids). Fig. 8 shows the relative intensity I_2 of this component as a function of the number of HPT turns.

The lifetime of positrons trapped in vacancy clusters increases with increasing size of cluster. Ab initio calculations of the lifetime of positrons trapped in vacancy clusters of various sizes in Cu performed in Ref. [8] make it possible to determine the mean size of vacancy clusters in HPT-deformed samples from the lifetime τ_2 . Fig. 9 shows the dependence of the mean size of vacancy clusters (expressed as the number of vacancies N_{VC} in the cluster) on the number of HPT turns. Vacancy clusters at the center consist of 4–5 vacancies, i.e. they are smaller than the clusters at the periphery, which consist of 7–9 vacancies. No significant change in the size of vacancy clusters with increasing number of HPT turns was observed.

Since vacancies in Cu become mobile below room temperature [26], it is expected that vacancies created during HPT processing either disappear by diffusion to sinks or agglomerate into small clusters. These clusters are responsible for the component with the lifetime τ_2 detected in the

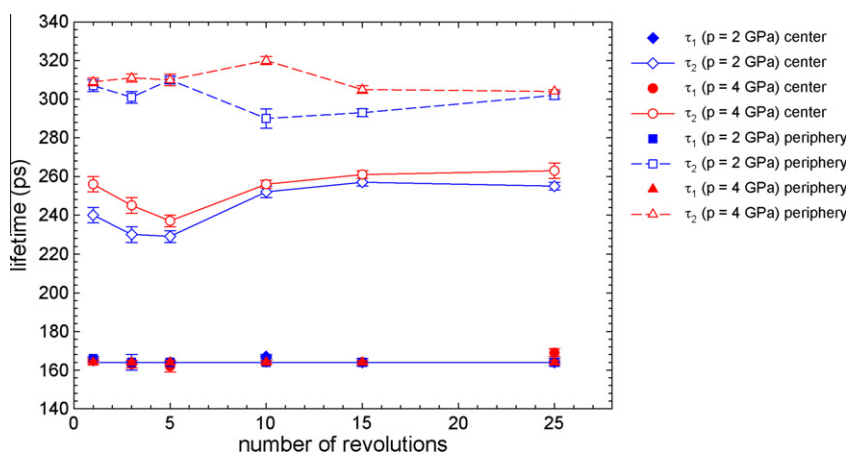


Fig. 7. Lifetimes τ_1 (full symbols) and τ_2 (open symbols) of the exponential components resolved in LT spectra of HPT-deformed samples plotted as a function of the number of HPT revolutions performed using pressures of 2 and 4 GPa. The lifetimes measured in the center of each sample ($r = 0$) and at the periphery ($r = 3 \text{ mm}$) are compared in the figure.

LT spectrum. Since there is competition between positron trapping at dislocations and in vacancy clusters, and deformed samples exhibit a high dislocation density, the appearance of the contribution from positrons trapped in vacancy clusters testifies to the very high concentration of vacancies in HPT-deformed samples. Indeed, vacancy clusters were detected in metals subjected to severe plastic deformation, e.g. HPT-deformed Cu [8,19,27], Ni [27,28] and Cu deformed by ECAP [29]. On the other hand, no vacancy clusters were detected in conventionally cold-rolled Cu [25]. From inspection of the PAS results shown in Figs. 7–9, one can draw the following conclusions:

- (i) There is always a significant difference between the center of the sample ($r = 0$) and the periphery ($r = 3$ mm). In particular, the peripheral region con-

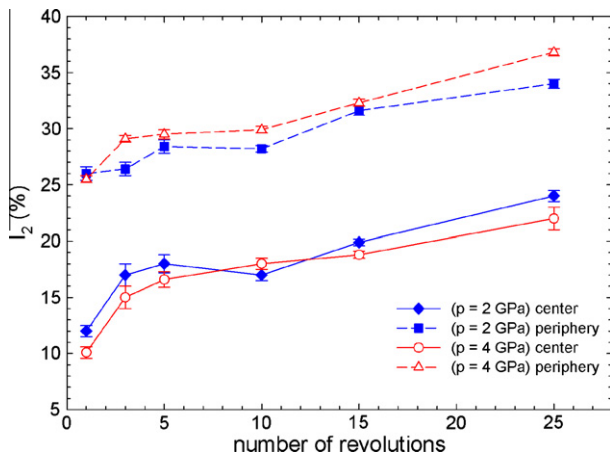


Fig. 8. The relative intensity I_2 of the component representing a contribution of positrons trapped in small vacancy clusters plotted as a function of number of HPT revolutions. Results measured in the center ($r = 0$) and at the periphery ($r = 3$ mm) are compared in the figure.

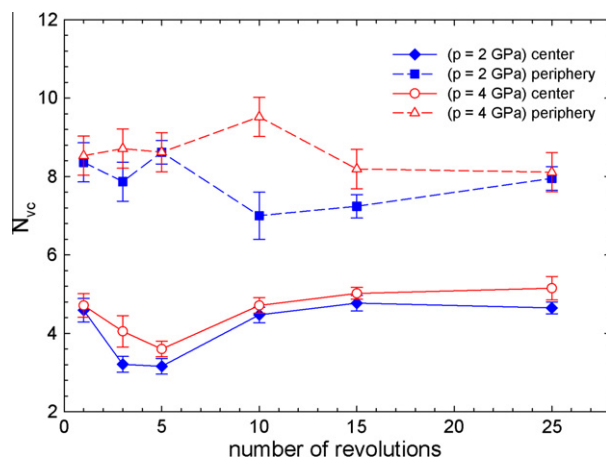


Fig. 9. The mean size of vacancy clusters (expressed as the average number of vacancies N_{VC} in the cluster) at the center and at the periphery of HPT-deformed samples.

tains larger vacancy clusters than the central region and has a higher contribution of positrons trapped in vacancy clusters.

- (ii) The intensity I_2 increases during HPT processing. Hence, the contribution of positrons trapped in vacancy clusters increases with increasing number of HPT turns.
- (iii) The samples deformed under pressures of 2 and 4 GPa exhibit very similar results.

3.5. Estimation of defect densities

No free positron component could be resolved in the LT spectra of HPT-deformed samples. This testifies to the very high density of defects. Already after the first HPT revolution defect density in the sample becomes so high that every positron is very quickly trapped at some defect (saturated positron trapping). The ratio I_2/I_1 of the relative intensities of positrons trapped in vacancy clusters and in dislocations is plotted in Fig. 10. Because of the saturated positron trapping, the ratio of intensities is directly proportional to the ratio of defect concentrations:

$$\frac{I_2}{I_1} = \frac{v_{VC}c_{VC}}{v_D\rho_D} \quad (2)$$

Here c_{VC} denotes the concentration of vacancy clusters and ρ_D stands for the dislocation density. The symbols v_{VC} and v_D denote the specific positron trapping rate to vacancy clusters and dislocations, respectively. The specific positron trapping rate for a small vacancy cluster consisting of N_{VC} vacancies ($N_{VC} \leq 10$) is proportional to the number of vacancies $v_{VC} = N_{VC}v_V$, where $v_V = (1.2 \pm 0.2) \times 10^{14}$ at s^{-1} [30] is the specific positron trapping rate for vacancy in Cu. The specific positron trapping rate for dislocations in Cu $v_D = 0.6 \times 10^{-4} m^2 s^{-1}$ was estimated in Ref. [31]. Using Eq. (2) and the dislocation density ρ_D determined by

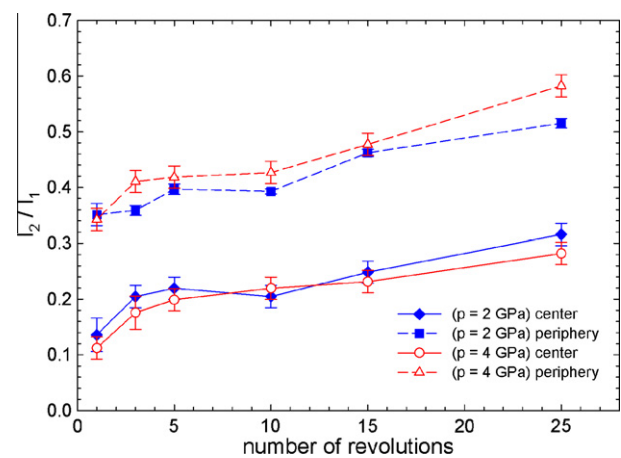


Fig. 10. The ratio I_2/I_1 of intensities of positrons trapped in vacancy clusters and positrons trapped at dislocations plotted as a function of the number of HPT revolutions. Results measured in the center of each sample ($r = 0$) and at the periphery ($r = 3$ mm) are compared in the figure.

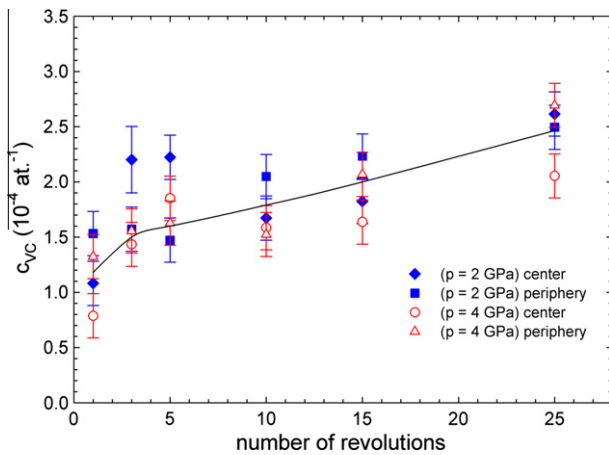


Fig. 11. The concentration of vacancy clusters c_{VC} calculated using Eq. (3) plotted as a function of the number of HPT revolutions. Results measured in the center of each sample ($r=0$) and at the periphery ($r=3$ mm) are compared in the figure. The solid line is only a visual guide.

XRD line-profile analysis, one can estimate the concentration of vacancy clusters in an HPT-deformed sample:

$$c_{VC} = \frac{I_2}{I_1} \frac{v_D}{N_{VC} v_V} \rho_D \quad (3)$$

Fig. 11 shows the concentration of vacancy clusters calculated using Eq. (3) as a function of the number of HPT revolutions. The concentration of vacancy clusters is similar in the samples deformed using pressures of 2 and 4 GPa. Moreover, the concentration of vacancy clusters at the center and at the periphery is comparable. However, the size of vacancy clusters at the periphery is roughly twice that at the center. The concentration of vacancy clusters increases with the number of HPT revolutions from 1.0 to $2.5 \times 10^{-4} \text{ at}^{-1}$. Note that a comparable concentration of vacancy clusters falling in the range $(1.5\text{--}4.5) \times 10^{-4} \text{ at}^{-1}$ was estimated from DSC data in Ref. [24] in Cu subjected to HPT deformation under pressures of 4 and 8 GPa.

Since vacancy clusters were formed by agglomeration of vacancies, one can estimate the concentration of vacancies in the sample simply as

$$c_V = N_{VC} c_{VC} = \frac{I_2}{I_1} \frac{v_D \rho_D}{v_V} \quad (4)$$

The concentration of vacancies obtained using Eq. (4) is plotted in Fig. 12 as a function of the number of HPT revolutions. The periphery exhibits enhanced concentration of vacancies due to larger size of vacancy clusters. The concentration of vacancies at the center of the sample as well as at the periphery increases with increasing number of HPT revolutions. This result testifies that the concentration of vacancies increases with increasing strain. Similar behavior was observed in Ref. [24]. The estimated concentration of vacancies in HPT-deformed Cu falls in the interval $(0.4\text{--}2.0) \times 10^{-3} \text{ at}^{-1}$. This concentration of vacancies is higher

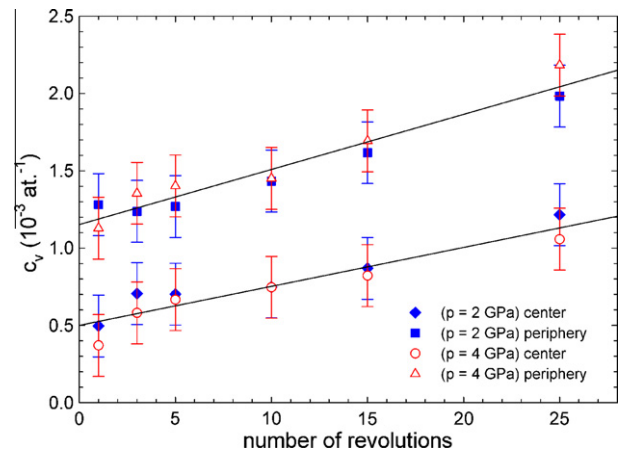


Fig. 12. The concentration of vacancies which formed vacancy clusters estimated using Eq. (4) plotted as a function of the number of HPT revolutions. Results measured in the center of each sample ($r=0$) and at the periphery ($r=3$ mm) are compared in the figure.

than the $c_V \approx (1\text{--}4) \times 10^{-4} \text{ at}^{-1}$ estimated in Cu deformed by ECAP [11]. It should be emphasized that Fig. 12 shows vacancies which agglomerated into vacancy clusters. This is only a fraction of the total number of vacancies created during plastic deformation because some vacancies disappeared by diffusion to sinks at GBs or were annihilated by climbing dislocations. The total concentration of vacancies c_{tot} generated by plastic deformation is proportional to the plastic work applied to the material [32]:

$$c_{tot} \approx \frac{A_V}{G} \int_0^\epsilon \tau d\gamma \quad (5)$$

Here τ is the shear stress, γ is the strain and $G = 48.3$ GPa [33] is the shear modulus for Cu. The factor $A_V \sim 10^{-2}$ [34] represents the fraction of the plastic work stored in vacancies. Substitution of Eq. (1) into Eq. (5) assuming maximum shear stress $\tau = Mr/I$, where $M \approx 5$ Nm is torque and $I = \pi R^4/2 \approx 640 \text{ mm}^4$ is the polar moment of inertia of the sample disk with diameter R , yields a rough estimation of the net concentration of vacancies:

$$c_{tot} \approx \frac{A_V}{G} \frac{4Mr^2}{R^4 h} N \quad (6)$$

The total concentration of vacancies created by plastic deformation at the periphery ($r=3$ mm) of the Cu specimens subjected to 1 and 25 HPT turns, respectively, estimated by Eq. (6), is $c_{tot} \approx 0.2$ and $8.0 \times 10^{-3} \text{ at}^{-1}$. These values are of a similar order of magnitude as experimental values (see Fig. 12), taking into account that Eq. (6) can give only a very rough estimate. Obviously some deformation-induced vacancies disappeared by diffusion into sinks at GBs or were annihilated by climbing dislocations. This effect is more pronounced at higher numbers of HPT turns and leads to an actual increase in vacancy concentration in the HPT-deformed sample that is lower than that predicted by Eq. (6).

4. Conclusions

Two types of lattice defects were found in Cu subjected to HPT deformation: (i) a high density of dislocations of the order of $\sim 7 \times 10^{15} \text{ m}^{-2}$ and (ii) small vacancy clusters, which were formed by agglomeration of deformation-induced vacancies. This proves that a very high concentration of vacancies is created during HPT processing. Investigation of the spatial distribution of defects across the disk sample revealed that the center of the specimen is characterized by a coarser structure, smaller size of vacancy clusters (i.e. lower concentration of vacancies) and lower hardness compared to the periphery. This is due to the fact that strain caused by torsion increases with the distance from the center of the sample disk. The concentration of deformation-induced vacancies increases with increasing strain, which leads to the formation of larger vacancy clusters at the periphery.

Acknowledgements

This work was supported by the Academy of Science of Czech Republic (Project Nos. KAN300100801 and IAA101120803) and by the Ministry of Education, Youths and Sports of the Czech Republic through the Research Plan No. MSM 0021620834.

References

- [1] Valiev RZ, Islamgaliev RK, Alexandrov IV. *Prog Mater Sci* 2000;45:103.
- [2] Valiev RZ, Korznikov AV, Mulyukov RR. *Mater Sci Eng A* 1993;168:141.
- [3] Valiev RZ, Musalinov RS, Tsenev NK. *Phys Status Solidi (a)* 1989;1115:451.
- [4] Valiev RZ, Alexandrov IV, Islamgaliev RK. In: Chow GM, Noskova NI, editors. *Nanocrystalline materials: science and technology*. Dordrecht: Kluwer; 1998. p. 121.
- [5] Zhilyaev AP, Langdon TG. *Prog Mater Sci* 2008;53:893.
- [6] Hautojärvi P. In: Hautojärvi P, editor. *Positrons in solids*. Berlin: Springer-Verlag; 1979. p. 1.
- [7] Islamgaliev RK, Chmelík F, Kužel R. *Mater Sci Eng A* 1997;237:43.
- [8] Čížek J, Procházka I, Cieslar M, Kužel R, Kuriplach J, Chmelík F, et al. *Phys Rev B* 2002;65:094106.
- [9] Oberdorfer B, Steyskal E-M, Sprengel W, Puff W, Pikart P, Hugenschmidt Ch, et al. *Phys Rev Lett* 2010;105:146101.
- [10] Ungár T, Schafner E, Hanák P, Bernstorff S, Zehetbauer MJ. *Mater Sci Eng A* 2007;462:398.
- [11] Schafner E, Steiner G, Korznikova E, Kerber M, Zehetbauer MJ. *Mater Sci Eng A* 2005;410–411:169.
- [12] Zehetbauer MJ, Kohout J, Schafner E, Sachslehner F, Dubravina A. *J Alloys Compd* 2004;378:329.
- [13] Horita Z, Langdon TG. *Mater Sci Eng A* 2005;410–411:422.
- [14] Zhilyaev AP, Lee S, Nurislamova GV, Valiev RZ, Langdon TG. *Scripta Mater* 2001;44:2753.
- [15] Zhilyaev AP, Nurislamova GV, Kim BK, Baró MD, Szupnar JA, Langdon TG. *Acta Mater* 2003;51:753.
- [16] Estrin Y, Molotnikov A, Davies CHJ, Lapovok R. *J Mech Phys Solids* 2008;56:1186.
- [17] Tian YZ, An XH, Wu SD, Zhang ZF, Figueiredo RB, Gao N, et al. *Scripta Mater* 2010;63:65.
- [18] Kawasaki M, Figueiredo RB, Langdon TG. *Acta Mater* 2011;59:308.
- [19] Čížek J, Procházka I, Brauer G, Anwand W, Kužel R, Cieslar M, et al. *Phys Status Solidi (a)* 2003;195:335.
- [20] Bečvář F, Čížek J, Lešák L, Novotný I, Procházka I, Šebesta F. *Nucl Instrum Methods A* 2000;443:557.
- [21] Matěj Z, Kužel R, Nichtová L. *Powder Diffract* 2010;25:125.
- [22] Matěj Z, Kužel R. Program/library for microstructure analysis by powder diffraction (MSTRUCT); 2009. <<http://xray.cz/mstruct/>>.
- [23] Favre-Nicolin V, Černý R. *J Appl Crystallogr* 2002;35:734.
- [24] Setman D, Schafner E, Korznikova E, Zehetbauer MJ. *Mater Sci Eng A* 2008;493:116.
- [25] McKee BTA, Saimoto S, Stewart AT, Scott MJ. *Can J Phys* 1974;52:759.
- [26] Mantl S, Trifhüser W. *Phys Rev B* 1978;17:1645.
- [27] Würschum R, Greiner W, Valiev RZ, Rapp M, Sigle W, Schneeweiss O, et al. *Scripta Metal Mater* 1991;25:2451.
- [28] Čížek J, Procházka I, Cieslar M, Stulíková I, Chmelík F, Islamgaliev RK. *Phys Status Solidi (a)* 2002;191:391.
- [29] Kužel R, Janeček M, Matěj Z, Čížek J, Dopita M, Srba O. *Metal Mater Trans* 2010;41A:1174.
- [30] Kluin JE, Hehenkamp Th. *Phys Rev B* 1991;44:11597.
- [31] Čížek J, Procházka I, Vostrý P, Chmelík F, Islamgaliev RK. *Acta Phys Polym A* 1999;95:487.
- [32] Kovacs I, Zsoldos L. *Dislocations and plastic deformations*. Amsterdam: Elsevier; 1973.
- [33] Humphreys FJ, Hatherly M. *Recrystallization and related annealing phenomena*. Oxford: Pergamon Press; 2004.
- [34] Zehetbauer M. *Key Eng Mater* 1994;97–98:287.